Comparison of Experimental Results and Numerical Predictions of Drop Diameter from a Single Submerged Nozzle in a Liquid–Liquid System

Faik A. Hamad[1], Mohammed K. Khan[1], Barbara K. Pierscionek[2] and Hans H. Bruun[1]*

[1]Department of Mechanical and Medical Engineering, University of Bradford, Bradford, Bradford BD7 1DP, UK
[2]Department of Biomedical Sciences, University of Bradford, Bradford BD7 1DP, UK

The determination of heat and mass transfer across liquid–liquid interfaces is a common design problem in many chemical processes. One of the key factors in determining the heat and mass transfer rates in such processes is the interfacial area of the liquid–liquid phases. Consequently, drop formation has been studied by many researchers because of its important effect on the transport rates (ie. high ratios of interfacial area to volume are obtained through formation of droplets of one liquid in the other). The size and uniformity of such droplets are two important factors, which have a significant impact on the transfer rates.

Drop and bubble formation from a single submerged nozzle have been studied by many researchers. The main features can be characterized into two categories: i) formation under constant pressure, when the pressure drop across the nozzle is very small (e.g. Davidson and Schuler, 1960); and ii) formation under constant flow rate when the pressure difference across the nozzle is high (e.g. Davidson and Schuler, 1960; Ramakrishnan et al., 1969; Kumar and Kuloor, 1970; and Geary and Rice, 1991). Most investigations have been carried out under a constant flow rate condition, because a simple force balance equation can be used in particular for gas–liquid flow without the complexity of the effect of gas pressure, which should be included in the first case.

This paper deals with forces acting during drop formation in a liquid–liquid system. There have been some notable contributions to bubble formation in gas–liquid systems such as e.g. Geary and Rice (1991), but this paper focuses on the special features, which apply to liquid–liquid systems.

The early work on drop formation by Harkins and Brown (1919) involved the calculation of drop volume at a very low flow rate by equating the buoyancy and interfacial forces. A correction for the fraction of liquid volume, which remains attached to the nozzle subsequent to drop break off, was incorporated. The work of Hayworth and Treybal (1950) extended the work of Harkins and Brown (1919) to cases where velocity effects became important. This was achieved by incorporating the inertia and drag forces caused by higher injection velocities into the force balance, resulting in a semi-empirical equation. Null and Johnson (1958) have also contributed to this field by proposing

*Author to whom correspondence may be addressed: E-mail address: h.h.bruun@bradford.ac.uk

This paper presents a comparison of experimental results and numerical predictions of drop formation from a single submerged nozzle for a liquid–liquid system. The theoretical model is a modification of previous models used for a two-stage drop formation mechanism. The model has been tested against experimental data for kerosene drop formation in distilled water using a range of different nozzle diameters. In addition, our liquid–liquid model has been compared with both experimental and predicted results from published literature. These comparisons demonstrate that for liquid–liquid systems, the present predictions of drop diameter versus dispersed phase nozzle velocity are in overall agreement with both the present and previous experimental results. In addition, the present model predictions are more accurate than those of previous models for liquid-liquid systems.

On présente dans cet article une comparaison entre des résultats expérimentaux et des prédictions numériques de formation des gouttes à partir d'un orifice submergé pour un système liquide–liquide. Le modèle théorique est une modification des modèles utilisés antérieurement pour décrire le mécanisme de formation de gouttes biphasique. Le modèle a été testé par rapport à des données expérimentales dans le cas de la formation de gouttes de kérosène dans de l'eau distillée pour une gamme de diamètres d'orifice. De plus, notre modèle liquide–liquide a été comparé à des données expérimentales et des résultats prédits provenant de la littérature scientifique. Ces comparaisons démontrent que pour des systèmes liquide–liquide les présentes prédictions de diamètre des gouttes en fonction de la vitesse de la phase dispersée à l'orifice concordent de manière acceptable avec les résultats expérimentaux présents et antérieurs. En outre, les prédictions du modèle actuel sont plus précises que celles des modèles précédents pour les sytèmes liquide–liquide.

Keywords: drop formation, diameter prediction, single nozzle, liquid–liquid system, transport phenomena.

a geometric approach to obtain a correlation for drop volumes at finite dispersed phase velocities. Both Hayworth and Treybal (1950) and Null and Johnson (1958) have attempted to model drop formation as a function of interfacial tension, continuous phase viscosity, nozzle diameter and the flow rate of the dispersed phase through the nozzle. Rao et al. (1966) developed a two-stage drop formation process to formulate their correlation. The drop was assumed to expand in the first (static) stage until the buoyant force balanced the interfacial tension force. Thereafter, in the second stage, the drop continued to grow until it became detached from the nozzle. Scheele and Meister (1968) and Chazal and Ryan (1971) have also presented a two-stage drop formation model for predicting the drop volume. Karagiannis et al. (1994) used four different diameter nozzles to study the size distribution of kerosene drops in stagnant distilled water under different flow rates. They found that their data could not be predicted by any of the above mentioned models (Hayworth and Treybal, 1950; Scheele and Meister, 1968; Chazal and Ryan 1971). A comprehensive review of work on both experimental and theoretical drop formation, which highlights the points mentioned earlier, has been carried out by Clift et al. (1978).

The experimental work of Hayworth and Treybal (1950), Null and Johnson (1958), Scheele and Meister (1968) and Chazal and Ryan (1971) show that the key factors which influence the drop size produced from nozzles are: interfacial tension; densities and viscosities of the two phases; the velocity of the dispersed phase through the nozzle; and the nozzle diameter. However, the previous studies also show that the correlations developed to predict the drop diameter depend on calibration factors determined from experimental data. Hence, they cannot be used to extrapolate beyond the experimental design parameters.

The objective of the present work was to formulate a model for the prediction of the drop diameter in liquid–liquid systems based on, in particular, the Geary and Rice (1991) model for a two-stage formation process for gas–liquid systems. The force balance analysis includes the forces of buoyancy, momentum, surface tension, drag and inertia in both stages. The results from the present model have been compared with both current kerosene–water flow experiments and with findings from aforementioned experimental and theoretical studies for a range of liquid–liquid system parameters.

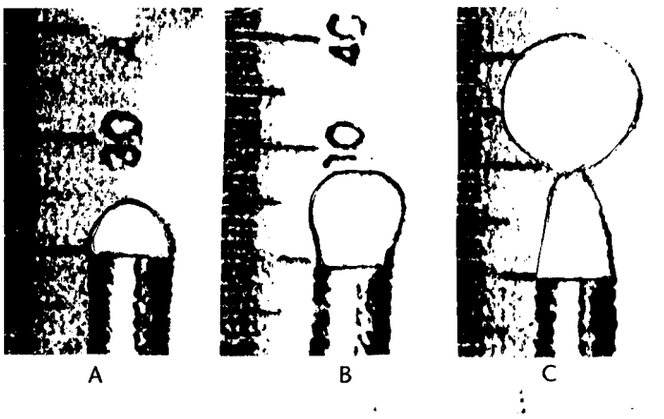

Figure 1a. Drop formation stages: A. Drop birth; B. Drop at the end of the first stage; C. Drop detachment at the end of the second stage.

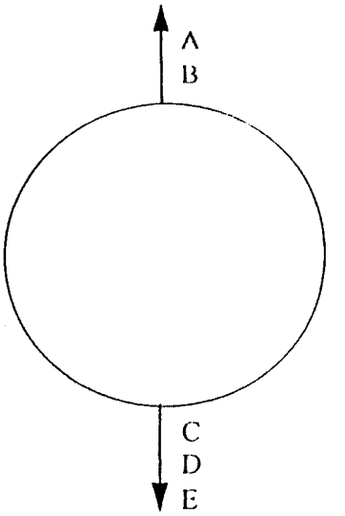

Figure 1b. Forces acting on the drop during both stages of formation: A. Buoyancy force; B. Momentum force; C. Surface tension force; D. Drag force; E. Inertia force.

The Liquid–Liquid Drop Formation Model

The drop formation is considered to take place in two stages as shown in Figure 1a. The related forces are indicated in Figure 1b. The drop growth during the first stage results in the formation of a near spherical drop which continues to grow until force balance, when the upward forces (buoyancy force (A) and momentum force (B)), are in balance with the downward forces (surface tension force (C), drag force (D) and inertia force (E)). In the model developed, the drop volume at the end of stage 1 decreases with increasing dispersed phase nozzle velocity. This is attributed to the inclusion of the momentum force, which results in a force balance before the drop reaches the 'static' drop volume (the volume of the drop at very low flow rate). Consequently, the limitation of the Rao et al. (1966) model to predict only a drop volume greater than the 'static' drop volume has been overcome. The calculated stage 1 drop volume is then taken as the starting point for the second stage drop volume evaluation. This stage (drop growth after force balance) starts when the upward forces are greater than the downward forces and the drop starts to move away from the nozzle. The drop will not lose its contact with the nozzle during this stage and the dispersed phase will continue to flow into the drop and its detachment tail (see Figure 1a) during this stage. As the drop volume increases, the drop accelerates and the break-off from the nozzle takes place when the drop has moved a distance x_m. The variation in x_m with nozzle diameter D_n is described later in this paper.

Stage-1 Drop Growth Until Force Balance

The balance of the forces which governs the drop formation (see Figure 1b) toward the end of stage-1 (Rao et al., 1966; Ramakrishnan et al., 1969; Heertjes et al., 1971; and Geary and Rice., 1991) can be written as:

Buoyancy force + Momentum force – Surface tension force – Drag force = Inertia force

Applying the concepts and notations introduced for drop formation in a liquid (Scheele and Meister, 1968) and for gas bubble formation in a liquid (Geary and Rice, 1991) to the drop formation of one liquid in another liquid, we obtain:

$$(\rho_c - \rho_d)Vg + \frac{Q^s \rho_d}{\pi R_n^2} - 2\pi\sigma R_n - F_D = \frac{d}{dt}(mVU_{d1}) \quad (1)$$

A major difference between gas–liquid and liquid–liquid systems is that the latter contains the density difference $(\rho_c - \rho_d)$ in the buoyancy force. Also using the coefficient of virtual mass, $m = \rho_d + \alpha\rho_c$ where $\alpha = 1/2[1+(3r^3/8s^3)]$ with s being the distance from the centre of the sphere to the wall and r being the radius of the sphere (Lamb, 1932), it follows that $\alpha \approx 1/2$ as our nozzle was raised 40 mm above the bottom of the test section, and therefore that the virtual mass coefficient $m \approx (\rho_d + 0.5\rho_c)$.

Assuming a spherical drop shape and that the average velocity of the drop is equal to the velocity of the drop centre, the drag force F_D, which is Reynolds number dependent as discussed by Stokes (1901) and Kunii and Levenspiel (1969), can, as identified in, e.g., Null and Johnson (1958), Rao et al. (1966) and Geary and Rice (1991), be expressed as:

$$Re < 1 \qquad F_D = 6\pi\mu_c r U_{d1} \quad (2a)$$

$$1 \le Re \le 500 \qquad F_D = 5\pi\sqrt{\frac{\rho_c\mu_c}{2}}(rU_{d1})^{3/2} \quad (2b)$$

As the Reynolds number Re >1, Equation (2b) will be used in this investigation.

With these modifications and using the inertia force derivations as described by Ramakrishnan et al. (1969), Kumar and Kuloor (1970) and Geary and Rice (1991), it can be shown that the force balance Equation at the end of the first stage, can be rewritten as:

$$\frac{4\pi}{3}(\rho_c - \rho_d)gr^3 + \frac{Q^2\rho_d}{\pi R_n^2} - 2\pi\sigma R_n - 5\pi\sqrt{\frac{\rho_c\mu_c}{2}}(rU_{d1})^{3/2} = \frac{mQ^2}{12\pi r^2} \quad (3)$$

Equation (3) can be solved iteratively to calculate the drop diameter d_1 at the end of stage 1.

Stage 2 Drop Growth During Detachment Stage

Drop growth continues to take place during stage 2 due to the additional volume flow into the drop and its detachment tail, until the time of detachment. During stage 2 the various force terms can be expressed as:

$$(\rho_c - \rho_d)Vg + \frac{Q^2\rho_d}{\pi R_n^2} - 2\pi\sigma R_n - 5\pi\sqrt{\frac{\rho_c\mu_c}{2}}(rU_{d2})^{3/2} = \frac{d}{dt}(mVU_{d2}) \quad (4)$$

Compared with stage 1, the following changes are made to the drag and inertia terms. As discussed by e.g. Ramakrishnan et al. (1969) and Kumar and Kuloor (1970) during stage 2 the drop velocity U_{d2} is a combination of drop rise away from the nozzle exit dx/dt and the drop expansion dr/dt:

$$U_{d2} = dx/dt + dr/dt \quad (5)$$

Equation (5) for the drop velocity U_{d2} is used in the inertia term and for simplicity U_{d2} is approximated by the expansion term dr/dt only in the drag term as suggested by Geary and Rice (1991).

Substituting Equation (5) in Equation (4) for the inertia term and as $d/dt(mVdr/dt) = mQ^2/12\pi r^2$ from stage 1 we get:

$$(\rho_c - \rho_d)Vg + \frac{Q^2\rho_d}{\pi R_n^2} - 2\pi\sigma R_n - 5\pi\sqrt{\frac{\rho_c\mu_c}{2}}(rU_{d2})^{3/2} - \frac{mQ^2}{12\pi r^2} = \frac{d}{dt}\left(mV\frac{dx}{dt}\right) \quad (6)$$

For the stage 2 process, indices 1 and 2 will refer to the conditions at the end of stage 1 and stage 2, respectively.

Assuming that all fluid flows into the drop during detachment, we have for a spherical drop growth:

$$V = V_1 + QT = \frac{4}{3}\pi r^3(T) \quad (7)$$

where $T = 0$ at the end of stage 1, and $T = T_2$ at the end of stage 2, and during stage 2, $T = t - t_1$ so that $d/dT = d/dt$.

Consequently, rewriting Equation (6) in terms of drop volume and integrating twice following a procedure similar to Geary and Rice (1991) it can be shown that:

$$\frac{A}{4Q^2}(V_2^2 - V_1^2) + B\left[\frac{(V_2 - V_1)}{Q^2} - \frac{V_1}{Q^2}\ln\left(\frac{V_2}{V_1}\right)\right] - \frac{4C}{Q^2}\left(V_2^{1/2} - V_1^{1/2}\right) - \frac{9D}{Q^2}\left(V_2^{1/3} - V_1^{1/3}\right) - \frac{E}{Q}\ln\left(\frac{V_2}{V_1}\right) = x_m \quad (8)$$

with

$$A = \frac{(\rho_c - \rho_d)g}{m}, B = \frac{\left(\frac{Q^2\rho_d}{\pi R_n^2} - 2\pi\sigma R_n\right)}{m}, C = \frac{5\sqrt{\rho_c\mu_c/6}Q^{3/2}}{4m}, D = \frac{Q^2}{12\pi(3/4\pi)^{2/3}}$$

and

$$E = \frac{A}{2Q}V_1^2 - \frac{2C}{Q}V_1^{1/2} - \frac{3D}{Q}V_1^{1/3}$$

Equation (8) can be solved iteratively for V_2 and therefore d_2 using the variation in x_m with nozzle diameter D_n described in the following section.

Experimental Procedure

Significant drop volume experimental data exists in the literature (Hayworth and Treybal, 1950; Null and Johnson, 1958; Rao et al., 1966; Scheele and Meister, 1968). Selected data have been used for comparison with the results of the present study. It was also considered prudent to carry out new experiments to obtain a better understanding of the drop formation and to use the experimental data for comparison with the model developed. In the present experiments, kerosene (ρ = 807 kg/m^3, supplier data, and σ = 0.030 N/m, Karagiannis et al., 1994) was used as the dispersed phase and distilled water was used as the continuous phase. These two liquids were chosen because they have been used extensively in collaborative research activities related to subsea oil recovery industries. Particular attention was paid to contaminants (and hence cleanliness) in the system, since these adversely change the interfacial tension.

Figure 2 illustrates the experimental apparatus used in this study. The dispersed phase (kerosene) was fed by gravity from a reservoir located approximately 3.0 m above the drop forming test sections. The Plexiglas drop forming pipe section was 350 mm high with an 80 mm inner diameter (allowing observation and filming of the drop formation process and its subsequent progress). The free surface of the stationary continuous phase was

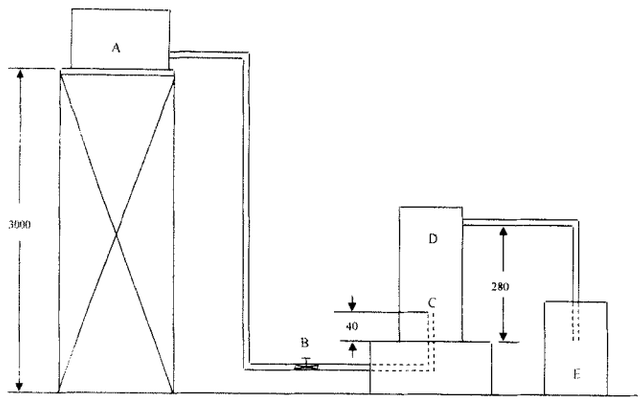

Figure 2. Experimental aparatus. A. Kerosene reservoir; B. Needle valve; C. Nozzle; D. Test section; E. Graduated cylinder. Dimensions in mm.

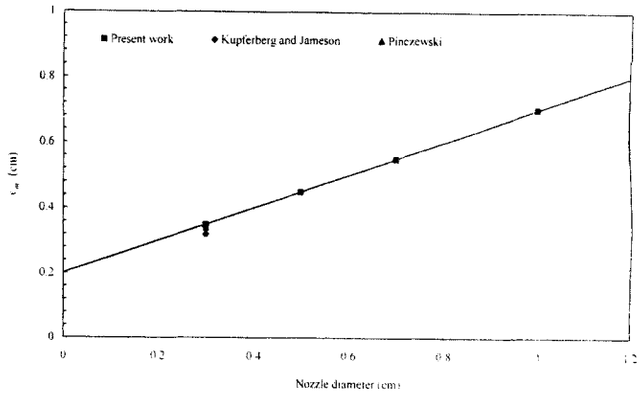

Figure 3. Variation in drop separation distance x_m with nozzle diameter D_n.

280 mm above the bottom of the test section. Four sharp-edge tip nozzles, with internal diameters of 0.3, 0.5, 0.7 and 1.0 cm were used in this study. Each nozzle protruded 40 mm from the bottom of the test section into the continuous phase giving a distance of 240 mm from the nozzle exit to the free surface of the continuous phase. Below each nozzle (and outside the test section) was a needle valve, used to accurately control the dispersed phase nozzle velocity and therefore the drop formation.

For each nozzle, the drop formation was recorded using a Sony CCD-TR350E video camera recorder (with an in-built timer), a video cassette recorder and a monitor. For each dispersed phase nozzle velocity, the video camera recorded the drops leaving the nozzle for a time period of 3 to 5 min. The drop formation experiment was then accurately studied using the video and monitor. By counting the drop numbers for a specific period of time (from a frame-by-frame video operation), the drop frequency was calculated. During the time period of the experiment, the dispersed phase was collected and measured in order to calculate the volume flow rate, Q. The experimental average drop volume (and diameter) was then calculated from the dispersed phase volume flow rate Q and the drop frequency. In addition the video recording clearly identified the drop formation process, confirming the establishment of near spherical drops during both stage 1 and stage 2 for nozzle diameters of 1.0 cm or less. These recordings also demonstrated that the drop formation process started close to the nozzle at low velocities while at moderate and high velocities the drop formation commenced from the top of a constant length detachment jet. For stage 2 it was observed from Figure 3, that the corresponding separation distance x_m varied linearly with nozzle diameter D_n as follows:

$$x_m = 0.5D_n + 2.0 \text{ (mm)} \qquad (9)$$

The separation distance for a nozzle of 0.3 cm was measured experimentally by Kupferberg and Jameson (1969) to be 0.32 cm and computed numerically by Pinczewski (1981) as being 0.34 cm, which is in good agreement with the experimentally observed value of 0.35 cm in this study.

Comparison of Experimental Results with Model Predictions

This section describes the comparison between the current kerosene–water drop formation experiments and the related model predictions.

Results for a 0.5 cm nozzle are described in Figure 4. This shows a comparison between: i) the measured final drop diameter d_2, and ii) from the model prediction: the calculated drop diameter at the end of stage 1, d_1, and the final drop diameter d_2; as a function of the dispersed phase nozzle velocity V_n. Experimental results and calculations compare well. It is noticed that the drop diameter d_1 during stage 1 decreases with increasing nozzle velocity V_n. However, in comparison, the figure also indicates that the increase in the drop diameter, $d_2 - d_1$, with nozzle velocity during stage 2 was faster than the decrease in d_1, resulting in an increase in d_2 with nozzle velocity. In general the shape of the final drop diameter curve $d_2(V_n)$ was found to depend on the interaction between these two opposing trends, which vary with nozzle size and with the liquid used.

Experimental tests and related model predictions were carried out with 4 nozzle sizes of the following diameters 0.3, 0.5, 0.7 and 1.0 cm. To illustrate the change in the drop size with both nozzle diameter D_n and dispersed phase nozzle

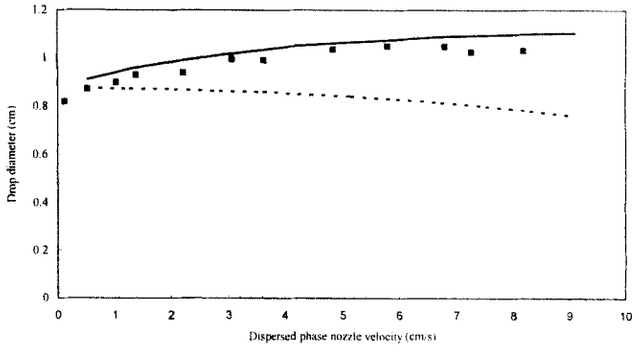

Figure 4. Variation of predicted drop diameter at the end of first stage d_1 (- - - -) and second stage d_2 (——) and experimental drop diameter (■) with dispersed phase nozzle velocity for nozzle diameter = 0.7 cm, kerosene–water.

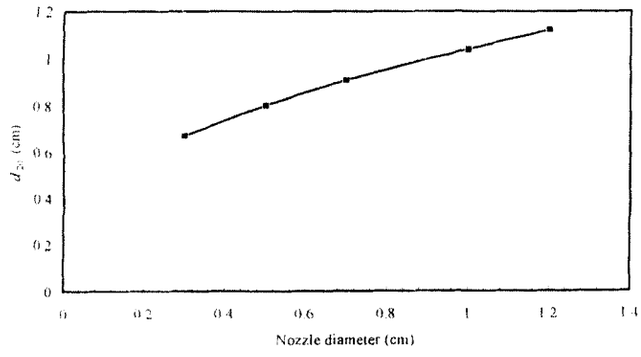

Figure 5a. Variation at very low nozzle velocity of calculated final drop diameter (d_{20}) with nozzle diameter, kerosene–water.

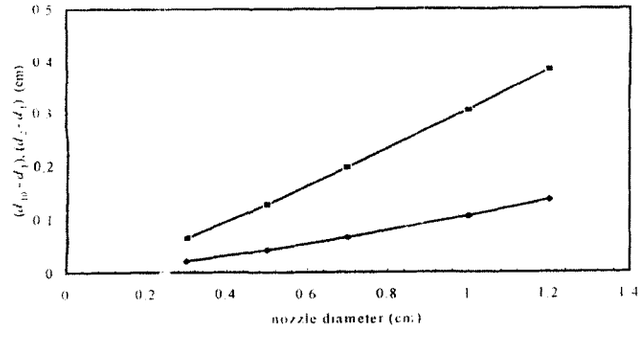

Figure 5b. Variation in the calculated decrease in stage 1 diameter ($d_{10} - d_1$), ■, and the increase in stage 2 diameter ($d_2 - d_1$) ,◆, with nozzle diameter, Nozzle velocity = 5cm/s, kerosene–water.

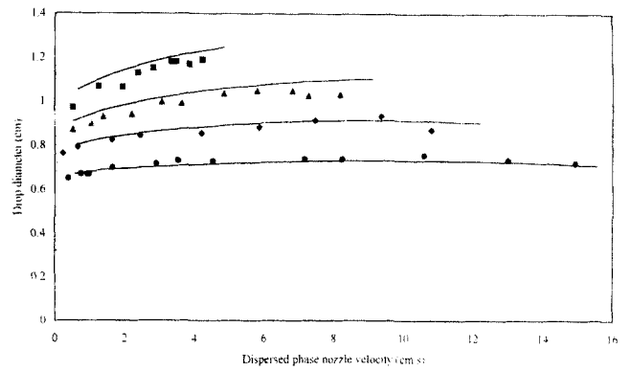

Figure 6a. Comparisons between experimental data for different nozzle diameters of •, 0.3 cm; ♦, 0.5 cm; ▲, 0.7 cm; ■, 1.0 cm and related model predictions (——) of final drop diameter, kerosene–water.

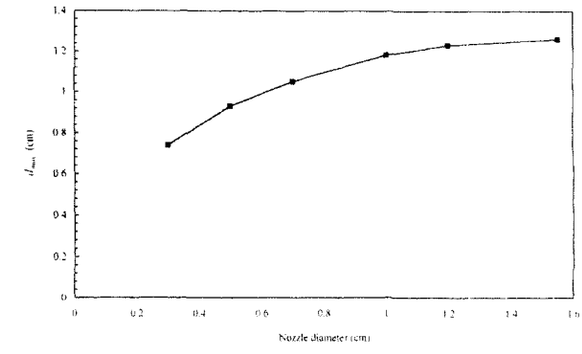

Figure 6b. Variation of the maximum drop diameter d_{max} with nozzle diameter D_n.

velocity V_n, the following summary features from the model predictions are presented in Figure 5. Figure 5a shows, for very low velocities, the variation in the final drop size d_{20} with nozzle diameter. It is clear that the drop diameter d_{20} increases linearly with the size of the nozzle diameter D_n. Figure 5b shows: i) the decrease with nozzle velocity in the drop diameter, $d_{10} - d_1$ during stage 1 (where d_{10} is the drop diameter at very low velocity); and ii) the corresponding increase in drop diameter, $d_2 - d_1$ during stage 2 of the drop formation process as a function of the nozzle diameter D_n for a dispersed phase nozzle velocity V_n of 5 cm/sec. From Figure 5b, it is evident that both the decrease in the drop diameter, $d_{10} - d_1$ during stage 1 and the increase in the drop diameter, $d_2 - d_1$ during stage 2 vary nearly linearly with the nozzle diameter. In general, it is observed that the increase in $d_2 - d_1$ with nozzle diameter is approximately three times as fast as the decrease in $d_{10} - d_1$. The net result is that the drop formation curves d_2 (V_n) attain increasingly positive slopes as the nozzle diameter is increased. This is confirmed by the drop formation curves in Figure 6a, which incorporate curves from experimental results together with model predictions covering the nozzle diameter range 0.3 to 1.0 cm. The two sets of data show good agreement with differences of less than 8%.

Figure 6b presents the variation of the maximum drop diameter d_{max} for each nozzle with nozzle diameter D_n. It was observed, as shown in Figure 6b that the difference in drop size between nozzle diameters of 1.2 and 1.55 cm was almost negligible and the maximum value was found to be about 12.6 mm. The physical explanation of the maximum drop size, in the case of a single drop rising with its terminal velocity, in a stagnant liquid without any disturbance on the interface, is as follows. The drop break-up will take place when its size exceeds the maximum stable drop size due to internal circulation. This causes a centrifugal force at the drop surface. When the centrifugal force is larger than the surface tension force, the drop will be stretched in an irreversible process until necking phenomenon occurs and the drop splits into two smaller drops. The maximum stable diameter has been studied by several researchers (e.g., Grace et al., 1978; Wilkinson et al., 1993; and Xukun et al., 1999) and was given in the general form of:

$$d_{max} = C\sqrt{\frac{\sigma}{g\Delta\rho}} \tag{10}$$

According to this formula, the maximum stable drop diameter d_{max} will vary directly with the surface tension σ and inversely with the density difference $\Delta\rho$. The value of the constant C is usually given as $C \approx 4$ (Grace et al., 1978; Wilkinson et al., 1993) for liquid drops. For kerosene drops in water, the numerical value of d_{max} is about 15.6 mm, which is higher than the

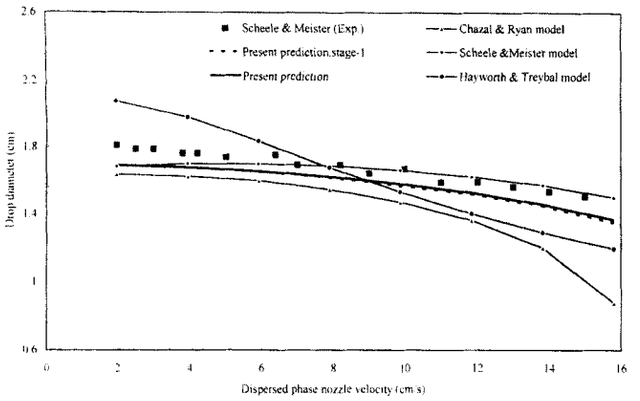

Figure 7. Model predictions and experimental data (from Scheele and Meister) of final drop diameter, 55% carbon tetachloride-45% heptane–water.

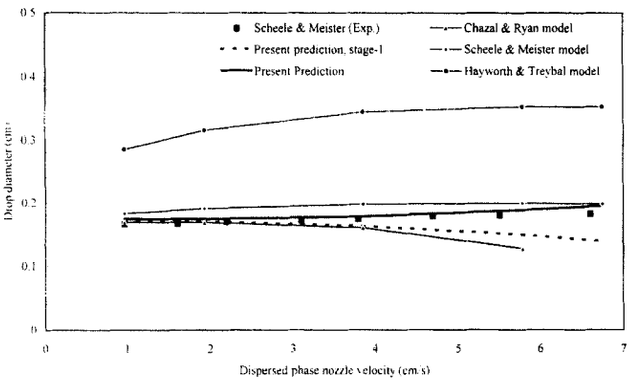

Figure 8. Model predictions and experimental data (from Scheele and Meister) of final drop diameter, butyl alcohol–water.

experimental results of 12.6 mm obtained in this investigation. The present finding is consistent with results in previous studies, which show that the experimental value is generally less than the predictions based on Equation (10) (Grace et al., 1978).

Comparison with Previous Results

The present modified model has been tested against previous experimental and related model predictions. The aim of the comparison was twofold: i) to demonstrate the good agreement between the predictions based on the modified model presented in this paper and previous experimental results; and ii) to highlight discrepancies observed using predictions based on previous models.

Three cases have been selected for comparison with our kerosene–water results, for which the surface tension was $\sigma = 0.030$ N/m and the density difference was $\Delta\rho = 193$ kg/m^3. These three cases cover significant variations in both σ and $\Delta\rho$:

i) 55% carbon tetrachloride–45% heptane–water, which has a very small density difference, $\Delta\rho = 10$ kg/m^3 and $\sigma = 0.032$ N/m (Scheele and Meister, 1968, data are presented in Figure 7 for $D_n = 0.254$ cm);

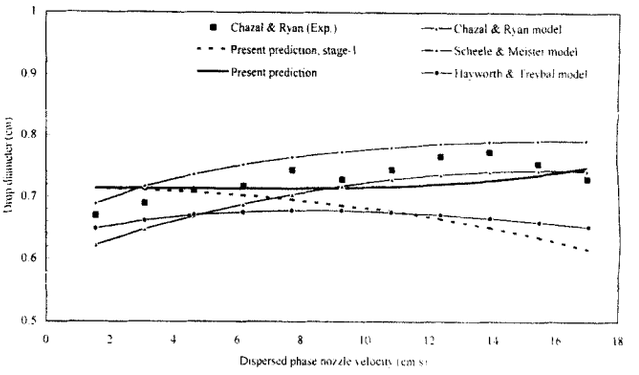

Figure 9. Model predictions and experimental data (from Chazal and Ryan) of final drop diameter, hexane–water.

ii) Butyl alcohol–water, which has a very small surface tension, $\sigma = 0.00179$ N/m and $\Delta\rho = 154$ kg/m^3 (Scheele and Meister, 1968, data are presented in Figure 8 for a small nozzle diameter $D_n = 0.0813$ cm);

iii) Hexane–water which has a high surface tension, $\sigma = 0.0495$ N/m, and a high density difference $\Delta\rho = 341$ kg/m^3 (Chazal and Ryan (1971) data are presented in Figure 9 for $D_n = 0.406$ cm).

These figures also include model predictions by: a) Scheele and Meister (1968); b) Chazal and Ryan (1971); c) Hayworth and Treybal (1950); and d) the present model showing both final drop diameter d_2 as well as stage 1 diameter d_1.

It is observed, from Figures 7 and 8, that for small values of $\Delta\rho$ or σ, both the Hayworth and Treybal (1950) and Chazal and Ryan (1971) models provide poor predictions. Scheele and Meister's model (1968) significantly over estimates the drop diameter when the values of $\Delta\rho$ and σ are both high (Figure 9).

Taking into account the substantial variations in the values of σ and $\Delta\rho$ in Figures 7 to 9, it can be concluded that, in general, the present predictions are in good agreement with the experimental results. The difference in trends between the predictions and experimental results at high nozzle velocity, shown in Figure 9, is most likely due to the approach of 'jetting' conditions. The results of the current predictions also show that the drop development during stage 1 and stage 2 depends substantially on the values of σ and $\Delta\rho$. For example, in Figure 7 in which the density difference is very small ($\Delta\rho = 10$ kg/m^3), the main drop development occurs during stage 1 with the final diameter d_2 being virtually identical to the drop diameter d_1 at the end of the stage 1 except at high nozzle velocities where a small difference is observed. In contrast, the largest difference between d_1 and d_2 occurs in Figure 9, where both σ and $\Delta\rho$ have substantially higher numerical values.

Conclusions

This paper presents a two-stage theoretical model, based on a modification of previous gas–liquid models, which predicts the drop diameter of the dispersed phase emanating from a submerged nozzle in a liquid–liquid system. By including the momentum force, which results in a physically more realistic earlier force balance, a new method for modelling the drop formation at the end of the first stage has been developed for liquid–liquid systems. The modified model has been used for comparative predictions of the variation in the drop diameter

with dispersed phase nozzle velocity utilizing experimental results for a kerosene–water mixture. The predicted results have also been compared with a number of experimental and predicted results from other related investigations. In general, it was shown that the present model provides better predictions than previous models because of a more realistic modelling of the physics of drop formation.

Acknowledgements

The principal author F.A. Hamad wishes to acknowledge an Iraqi government grant. Dr. H.H. Bruun wishes to acknowledge the award of an EPSRC grant and financial contribution by Schlumberger Cambridge Research Limited. Dr. B. Pierscionek wishes to acknowledge the award of an EPSRC grant (GR/M46310).

Nomenclature

d_1	drop diameter at the end of stage 1, (m)
d_{10}	drop diameter at the end of stage 1 for very low velocity, (m)
d_2	drop diameter at the end of stage 2, (m)
d_{20}	drop diameter at the end of stage 2 for very low velocity, (m)
d_{max}	maximum drop diameter, (m)
D_n	nozzle diameter, (m)
F_D	drag force, (N)
g	acceleration due to gravity, (m/s^2)
m	virtual mass coefficient
Q	flow rate of dispersed phase from the nozzle, (m^3/s)
r	drop radius at any time t, (m)
Re	drop Reynolds number
R_n	nozzle radius, (m)
T	time during stage 2, (s)
U_{d1}	drop velocity during stage 1, (m/s)
U_{d2}	drop velocity during stage 2, (m/s)
V	drop volume at any time t, (m^3)
V_1	drop volume at the end of stage 1, (m^3)
V_n	dispersed phase velocity at the nozzle outlet, (m/s)
x	distance from nozzle to the drop base, (m)
x_m	drop separation distance at the end of stage 2, (m)

Greek Symbols

μ_c	viscosity of continuous phase, (Pa·s)
ρ_c	density of continuous phase, (kg/m^3)
ρ_d	density of dispersed phase, (kg/m^3)
σ	surface tension coefficient, (N/m)

References

Clift, R., J.R. Grace and M.E. Weber, "Bubbles, Drop and Particles", Academic Press, New York, NY (1978).

Chazal, L.E.M. and J.T. Ryan, "Formation of Organic Drop in Water", AIChE J. **17**, 1226–1229 (1971).

Davidson, J.F. and O.G. Schuler, "Bubble Formation at an Orifice in a Viscous Liquid", Trans. Inst. Chem. Engrs. 38, 144–154 (1960).

Geary, N.W. and R.G. Rice, "Bubble Size Prediction for Rigid and Flexible Spargers", AIChE J. **37**, 161–168 (1991).

Grace, J.R., T. Wairgi and T.H. Nguyen, "Shapes and Velocities of Single Drops and Bubbles Moving Freely Through Immiscible Liquids", Trans. Inst. Chem. Engrs. **54**, 167–173 (1976).

Harkins, W.D. and F.E. Brown, "The Determination of Surface Tension (Free Surface Energy and the Weight of Falling Drops-Surface Tension of Water and Benzene by the Capillary Height Method)", J. Am. Chem. Soc. **41**, 499 (1919).

Hayworth, C.B. and R.E. Treybal, "Drop Formation in Two-Liquid-Phase Systems", Ind. Eng. Chem. **42**, 1174–1181 (1950).

Heertjes, P.M., L.H. de Nie and H.J. de Vries, "Drop Formation in Liquid–Liquid Systems–I. Prediction of Drop Volumes at Moderate Speed of Formation", Chem. Eng. Sci. **26**, 441–449 (1971).

Kumar, R. and N.R. Kuloor, "Bubbles Formation in Viscous Liquids Under Constant Flow Conditions", Can. J. Chem. Eng. **48**, 161–168 (1970).

Karagiannis, C., D. Papageorgiou and M. Stamatoudis, "Size Distribution of Drops formed from Nozzles in Liquid–Liquid Systems at Velocities below Jetting", Can. J. Chem. Eng. **72**, 13–15 (1994).

Kunii, D. and O. Levenspiel, "Fluidization Endineering", Wiley, New York, NY (1978).

Kupferberg, A. and G.J. Jameson, "Bubble Formation at a Submerged Orifice above a Gas Chember of Finite Volume", Trans. Instn. Chem. Engrs. **47**, 241–250 (1969).

Lamb, H., "Hydrodynamics", Cambridge University Press, Cambridge, UK (1932).

Mori, Y.H., "Harkins-Brown Correction Factor for Drop Formation", AIChE J. **36**, 1272–1274 (1990).

Null, H.N. and H.F. Johnson, "Drop Formation in Liquid–Liquid Systems from Single Nozzle", AIChE J. **4**, 273–281 (1958).

Pinczewski, W.V., "The Formation and Growth of Bubbles at a Submerged Orifice", Chem. Eng. Sci. **36**, 405–411 (1981).

Ramakrishnan, S., R. Kumar and N.R. Kuloor, "Studies in Bubble Formation I: Bubble Formation under Constant Flow Conditions", Chem. Eng. Sci. **24**, 731–747 (1969).

Rao, E.V.L.N., R. Kumar and N.R. Kuloor., "Drop Formation Studies in Liquid–Liquid Systems", Chem. Eng. Sci. **21**, 867–880 (1966).

Scheele, G.F. and B.J. Meister, "Drop Formation at Low Velocities in Liquid–Liquid Systems", AIChE J. **14**, 9–15 (1968).

Stokes, G.G., "On the Effect of the Internal Friction of Fluids on the Motion of Pendulums", Math. and Phys. Papers, Cambridge III, Cambridge, UK **55** (1901).

Wilkinson, P.M., A.V. Schayic, J.O.M. Spronken and L.L. Dierendonck, "The Influence of Gas Density and Liquid Properties on Bubble Break-up", Chem. Eng. Sci. **48**, 1213–1226 (1993).

Xukun, L., D.J. Lee, L. Raymond, Y. Guoqiang and F. Liang-Shih, "Maximum Stable Bubble Size and Gas Hold-up in High-Pressure Slurrey Bubble Columns", AIChE J. **45**, 665–680 (1999).

Manuscript received July 18, 2000; revised manuscript received April 17, 2001; accepted for publication April 23, 2001.